NASA
Technical
Paper
2675

January 1987

Revised NASA Axially Symmetric Ring Model for Coupled-Cavity Traveling-Wave Tubes

Jeffrey D. Wilson

NASA

NASA
Technical
Paper
2675

1987

Revised NASA Axially Symmetric Ring Model for Coupled-Cavity Traveling-Wave Tubes

Jeffrey D. Wilson

Lewis Research Center
Cleveland, Ohio

National Aeronautics
and Space Administration

Scientific and Technical
Information Branch

Summary

A versatile large-signal, two-dimensional computer program is used by NASA to model coupled-cavity traveling-wave tubes (TWT's). In this model, the electron beam is divided into a series of disks, each of which is further divided into axially symmetric rings which can expand and contract. The trajectories of the electron rings and the radiofrequency (RF) fields are determined from the calculated axial and radial space-charge, RF, and magnetic forces as the rings pass through a sequence of cavities. By varying electrical and geometric properties of individual cavities, the model is capable of simulating severs, velocity tapers, and voltage jumps. The calculated electron ring trajectories can be used in designing magnetic focusing and multidepressed collectors. The details of using the program are presented, and results are compared with experimental data.

Introduction

A one-dimensional computer model for a coupled-cavity traveling-wave tube was developed at NASA in the 1970's (refs. 1 and 2) and was used to design the traveling-wave tube for the NASA Communications Technology Satellite (CTS). In 1984, O'Malley (ref. 3) revised the model by simulating the electron beam with axially symmetric rings of electric charge which could expand or contract in the presence of a magnetic field. In the present study, the model has been further revised to allow (1) a tube with up to 200 cavities to be simulated, (2) magnetic pole pieces to be of different radii than the tunnel tips, and (3) magnetic periods to be independent of cavity periods in periodic permanent magnet (PPM) focusing designs. O'Malley referred to the model as three-dimensional since the electron rings travel in the axial direction, expand and contract in the radial direction, and rotate in the azimuthal direction. However, since the rings are axially symmetric and there is no azimuthal dependence, it is more accurate to refer to the model as two-dimensional.

In this model, the electron beam is divided into a series of disks, each of which is further divided into axially symmetric rings. The trajectories of the electron rings and the RF fields are determined from the calculated axial and radial space-charge, RF, and magnetic forces as the rings pass through a sequence of cavities. Each cavity has individually entered geometric and electrical parameters. This enables the model to simulate severs, voltage jumps, and velocity taper designs.

With the original one-dimensional model, Connolly and O'Malley (ref. 1) showed that the calculated small-signal gain as a function of frequency for the CTS TWT compared well with the experimental data. Even better agreement is expected with the two-dimensional model because the radial space-charge, RF, and magnetic forces can be simulated. Furthermore, modeling both the axial and the radial component of the electron beam trajectory is essential in designing magnetic focusing or a multidepressed collector at the tube output.

In this report, a description of the physical formulation of the model is reviewed, and the mechanics of utilizing the computer program are detailed and updated. The accuracy of the two-dimensional model is verified by comparing its results with those of the one-dimensional model and with the experimental data for the CTS coupled-cavity traveling-wave tube.

Symbols

a	tunnel radius
$\bar{a}$	inner radius of magnet stack
B	magnetic field
B_0	axial magnetic field at pole piece radius and midpoint of gap
b_0	initial beam radius
c	velocity of light
E	electric field
f	frequency
g	half-length of K^{th} magnetic gap
I_0	beam current
j	ring index (j = 1, 2, 3 refers to inner, middle, and outer ring)
L	cavity length
ℓ_K	half-length of K^{th} cavity gap
m	ring mass
$\bar{m}$	electric field shape parameter
N_c	number of cavities in TWT
N_d	number of disks in a beam wavelength
N_z	number of axial divisions in cavity

P magnetic period
$P_{f,K}$ average power flow in forward direction
P_{in} input power
q ring electric charge
R number of rings per disk
r centroid radius
$\dot{r}$ ring radial velocity
$r_{R,0}$ initial radius of outermost ring
$r_{\text{in},j}$ inner radius of j^{th} ring
$r_{\text{out},j}$ outer radius of j^{th} ring
$t_i(z_{n,k})$ time of arrival of i^{th} ring at axial position $z_{n,k}$
U relativistic factor
u beam velocity
$V_{b,K}$ backward propagating voltage in K^{th} cavity
V_K amplitude of voltage across gap in K^{th} cavity
$V_{f,K}$ forward propagating voltage in K^{th} cavity
V_0 beam voltage
$\Delta V_{b,K}$ backward induced voltage in K^{th} cavity
$\Delta V_{f,K}$ forward induced voltage in K^{th} cavity
v_p wave phase velocity
Z_K total interaction impedance for K^{th} cavity
z axial distance
$\dot{z}$ ring axial velocity
Δz_K length of axial division in K^{th} cavity, L_K/N_z
$\alpha + j\beta_1$ propagation constant
λ_e beam wavelength
$\bar{\mu}$ magnetic field shape parameter
$\dot{\varphi}$ ring azimuthal velocity
$\psi(r,z)$ axial magnetic flux through ring
ψ_c cathode flux at outermost ring
ω angular frequency

Subscripts

b backward
f forward
in inner
K,m cavity numbers
out outer
RF radiofrequency
r radial
SC space charge
VJ voltage jump
z axial
φ azimuthal
0 initial

Description of Model

The theory and mathematical derivation of the governing equations for the two-dimensional model is documented in detail by O'Malley (ref. 3). In this section, the procedure for the solution of these equations is reviewed and summarized.

Figure 1 illustrates the model. The electron beam is divided into a series of disks, each of which is divided into a maximum of four axially symmetric rings. The beam trajectory is described by following the rings contained in a single beam wavelength, which is equal to u_0/f, where u_0 is the initial beam velocity and f is the frequency of the RF signal. The axial thickness of all rings remains equal and constant at λ_e/N_d, where λ_e is the beam wavelength and N_d is the number of disks in a beam wavelength. The rings expand and contract radially and may penetrate each other in both the radial and axial directions. When the rings enter the tube they have the same charge and the same cross-sectional area. The axial and radial thickness of a ring is taken into account only in the modeling of beam interception and in the calculation of space-charge forces. For all other forces, it is assumed that the charge and mass of a ring are concentrated at the ring's centroid radius. The initial centroid radii are given by

$$r_j = \sqrt{\frac{2j-1}{2R}}\, b_0 \qquad j = 1,\ldots,R \tag{1}$$

where R is the number of rings per disk and b_0 is the initial beam radius. The inner and outer radii of the rings are given by

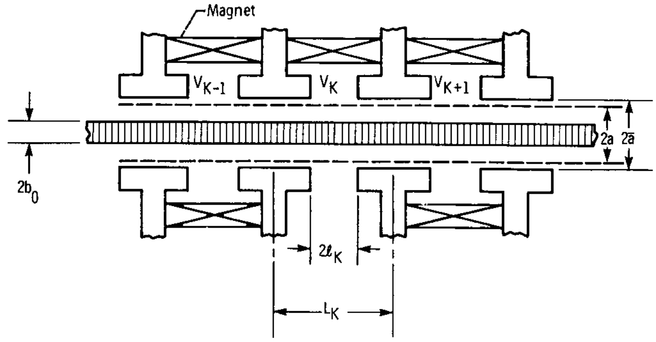

Figure 1.—Model of coupled-cavity traveling-wave tube.

$$r_{\text{in},j} = \sqrt{\frac{2j-2}{2j-1}}\, r_j \qquad j = 1,\ldots,R \tag{2}$$

$$r_{\text{out},j} = \sqrt{\frac{2j}{2j-1}}\, r_j \qquad j = 1,\ldots,R \tag{3}$$

Note that the inside "ring" is actually a disk; that is, its inner radius is zero.

The tube body is modeled as a conducting tunnel of radius a divided axially into a series of discrete cavities, where the length of the K^{th} cavity is L_K. In the center of each cavity is a gap of length $2\ell_K$. Impressed across the K^{th} gap is a complex voltage $V_K e^{j\omega t}$.

The procedure for calculating the electron beam trajectories and cavity voltages in the model is summarized in the following steps:

(1) The input data for the beam and cavities are read into the model. The details of entering the input parameters are presented in the next section.

(2) Space-charge tables are calculated. The space-charge force on a ring of centroid radius r_1 and electric charge q_1 due to a ring of centroid radius r_2 and electric charge q_2 located an axial distance z away is given by equations (39) to (41) of reference 3. Using these equations for calculating space-charge forces on each integration step would be very time consuming. Thus space-charge tables are calculated for discrete values of r_1, r_2, z, and j (j is the ring index; for example, if there are three rings per disk, j = 1, 2, and 3 refers to an inner, middle, and outer ring, respectively). During the computer simulation, the space-charge force on one ring due to another is calculated by using linear interpolation with the appropriate table.

(3) For the K^{th} cavity, tables of coefficients are calculated for the RF electric field, the voltage-jump electric field, and the beam-wave interaction field. These coefficients are evaluated for an array of r and z values and stored in tables when cavity K is entered. The tables are interpolated in a later step to calculate the forces.

In reference 3, the RF electric field coefficients are given by equations (59), (62), and (63); the voltage-jump coefficients by equations (74), (76), and (77); and the beam-wave interaction coefficients by equations (59) and (121).

(4) A first approximation for the induced voltage in cavity K due to the electron beam is calculated. The total induced voltage in the K^{th} cavity consists of a forward induced voltage component $\Delta V_{f,K}$, which propagates in the forward direction, and a backward induced voltage component $\Delta V_{b,K}$, which propagates in the backward direction. A first approximation to $\Delta V_{f,K}$ is obtained by assuming that the rings have constant velocities in the cavity. Thus

$$t_i(z_{n,K}) = t_i(z_{1,K}) + \frac{dt_i(z_{1,K})}{dz}(z_{n,K} - z_{1,K}) \qquad n = 1,\ldots,N_z \tag{4}$$

where $t_i(z_{n,K})$ is the time of arrival of the i^{th} ring at the axial position $z_{n,K}$ and $dt_i(z_{1,K})/dz = 1/\dot{z}(z_{1,K})$ is the reciprocal of the velocity of the i^{th} ring at the axial position $z_{1,K}$. The axial position is defined by

$$z_{n,K} = \sum_{m=0}^{K-1} L_m + \left(n - \frac{1}{2}\right)\Delta z_K \qquad \begin{cases} n = 1,\ldots,N_z \\ K = 1,\ldots,N_c \end{cases} \tag{5}$$

where N_z is the number of axial divisions in the cavity, N_c is the number of cavities in the TWT, L_m is the length of the m^{th} cavity, and Δz_K is the length of an axial division in the K^{th} cavity, where $\Delta z_K = L_K/N_z$. With the approximation of equation (4) the forward induced voltage $\Delta V_{f,K}$ is calculated from equations (126) and (127) of reference 3.

For a forward propagating wave in the passband of a uniform structure in the absence of the electron beam, Floquet's Theorem gives

$$V_{f,K} = e^{-(\alpha + j\beta_1)L} V_{f,K-1} \tag{6}$$

where $V_{f,K}$ is the forward propagating voltage in the K^{th} cavity, $\alpha + j\beta_1$ is the complex propagation constant, and L is the cavity length. When the voltage induced by the beam is added and the differences in impedances between cavities are taken, the forward propagating voltage is

$$V_{f,K} = \sqrt{\frac{Z_K}{Z_{K-1}}}\, V_{f,K-1} e^{-(\alpha L)_{f,K-1}} e^{-j(\beta_1 L)_{K-1}} + \Delta V_{f,K} \tag{7}$$

where the factor $\sqrt{Z_K/Z_{K-1}}$ ensures that power flow is conserved. In the first cavity $K = 1$,

$$V_{f,1} = \sqrt{2Z_1 P_{\text{in}}} + \Delta V_{f,1} \tag{8}$$

where Z_1 is the total interaction impedance and P_{in} is the input power.

(5) In this step, the ring trajectories are calculated from the equations of motion.

The axial and radial equations of motion are respectively

$$\frac{d^2z}{dt^2} = \beta\left\{\frac{q}{m}\left(E_{RF,z} + E_{SC,z} + E_{VJ,z} - r\dot{\varphi}B_r\right) + U_z\right\} \quad (9)$$

$$\frac{d^2r}{dt^2} = \beta\left\{\frac{q}{m}\left(E_{RF,r} + E_{SC,r} + E_{VJ,r} + r\dot{\varphi}B_z\right) + \frac{1}{\beta}r\dot{\varphi}^2 + U_r\right\} \quad (10)$$

where q is the ring electric charge; m is the ring mass;

$$\beta = \sqrt{1 - \frac{\dot{z}^2 + \dot{r}^2 + r^2\dot{\varphi}^2}{c^2}} \quad (11)$$

where c is the velocity of light;

$$\dot{\varphi} = \dot{\varphi}_0 - \frac{q}{m}\left[\frac{\psi(r,z) - \psi(r_0,z_0)}{2\pi r^2}\right]\beta \quad (12)$$

where $\psi(r,z)$ is the axial magnetic flux through the ring; B_z, B_r, and B_φ are axial, radial, and azimuthal components of the magnetic field, respectively; $E_{RF,z}$ and $E_{RF,r}$ are axial and radial RF electric field; $E_{VJ,z}$ and $E_{VJ,r}$ are axial and radial voltage-jump electric field; $E_{SC,z}$ and $E_{SC,r}$ are axial and radial space-charge electric field; and U_z and U_r are axial and radial relativistic factors.

The initial axial velocity for each ring in cavity $K = 1$ is

$$\dot{z}_0 = \sqrt{u_0^2 - \left(\frac{\sqrt{2}}{2}b_0\dot{\varphi}_0\right)^2} \quad (13)$$

where b_0 is the initial beam radius, and the initial beam velocity is

$$u_0 = c\sqrt{1 - \frac{1}{\left(1 + \frac{\left|\frac{q}{m}\right|V_0}{c^2}\right)^2}} \quad (14)$$

where c is the velocity of light, $|q/m|$ is the charge to mass ratio, and V_0 is the beam voltage. The initial azimuthal velocity of each ring is

$$\dot{\varphi}_0 = \frac{-\left|\frac{q}{m}\right|\psi_c}{2\pi r_{R,0}^2} \quad (15)$$

where ψ_c is the cathode flux at the outermost ring and $r_{R,0}$ is the initial radius of the outermost ring.

The cavity is divided into N_z equal parts of length Δz_K. By using finite differences with z as the independent variable, equations (9) and (10) are integrated to the end of the cavity. At the end of each integration step, the solution is checked for beam interception. If the outer radius of a ring exceeds the tunnel radius a, then the outer radius is redefined to be a, and the portion of the ring located beyond $r = a$ is assumed to be intercepted. The centroid radius for the remaining partial ring is redefined by

$$r_j = \sqrt{\frac{r_{in,j}^2 + r_{out,j}^2}{2}} \quad (16)$$

(6) After the beam ring trajectories have been calculated for a cavity, a better approximation to the induced voltage is obtained from equations (126) and (127) of reference 3. If the new value of $V_{f,K}$ differs from the old value by more than a predetermined amount (expressed by TOLDV in input), step 5 is repeated until the value converges. Then the backward induced voltage is calculated from equations (124) and (128) of reference 3. The $\Delta V_{b,K}$'s are stored for use in the next pass through the tube.

(7) Steps 3 through 6 are repeated for each cavity in succession to the end of the tube. If cavity $K + 1$ has the same input parameters as cavity K, the tables in step 3 do not need to be recalculated.

(8) After $\Delta V_{b,K}$ for the last cavity $K = K_2$ is calculated, the backward voltages are determined for all the cavities from the stored $\Delta V_{b,K}$'s. For the last cavity

$$V_{b,K_2} = \Delta V_{b,K_2} \quad (17)$$

Then proceeding backwards to the first cavity $K = 1$

$$V_{b,K} = \Delta V_{b,K} + V_{b,K+1}\sqrt{\frac{Z_K}{Z_{K+1}}}\,e^{-(\alpha L)_{b,K}}e^{-j(\beta_1 L)_K}$$

$$K = K_2 - 1,\ K_2 - 2,\ldots,1 \quad (18)$$

(9) After all the $V_{b,K}$'s have been calculated, a second pass is made through the tube. The second pass yields a new set of $\Delta V_{b,K}$ that can be used for calculating a set of $V_{b,K}$ for a third pass. As many passes as necessary to obtain convergence are performed.

Model Input

Three types of magnetic focusing fields can be modeled: (1) uniform solenoid focusing, (2) single-period periodic permanent magnetic (PPM) focusing, and (3) double-period PPM focusing.

For uniform solenoid focusing, the magnetic field is given by

$$B_z(r,z) = B_0 \tag{19}$$

$$B_r(r,z) = 0 \tag{20}$$

where the constant B_0 (B0) is a program input.

Figure 2 shows the geometry and axial magnetic field for single-period PPM focusing. The gap length between magnets is $2g$ (TWOGCM), the inner radius of the magnet stack is $\bar{a}$ (ABARCM), the magnetic period is P (LMAGCM), and the magnetic shaping factor is $\bar{\mu}$ (MU). The axial magnetic field at the pole piece radius and midpoint of the gap is B_0 (B0). The magnetic field components $B_z(r,z)$ and $B_r(r,z)$ are then given by

$$B_z(r,z) = \sum_{n=1}^{\infty} a_n I_0(k_n r)\cos(k_n z) \tag{21}$$

$$B_r(r,z) = \sum_{n=1}^{\infty} a_n I_1(k_n r)\cos(k_n z) \tag{22}$$

where $I_0(k_n r)$ and $I_1(k_n r)$ are modified Bessel functions,

$$k_n = \frac{2\pi}{P} \tag{23}$$

with P the magnetic period, and

$$a_n = \begin{cases} \dfrac{8B_0[\bar{\mu} \sinh \bar{\mu}g \cos k_n g + k_n \cosh \bar{\mu}g \sin k_n g]}{P\left(\bar{\mu}^2 + k_n^2\right) I_0(k_n \bar{a})}, & n \text{ odd} \\ 0, & n \text{ even} \end{cases} \tag{24}$$

Alternatively to entering $B_z(r,z)$ at $r = \bar{a}$, measured on-axis values $B_z(0,z)$ over a magnetic period can be entered (as the input parameter BZDATA).

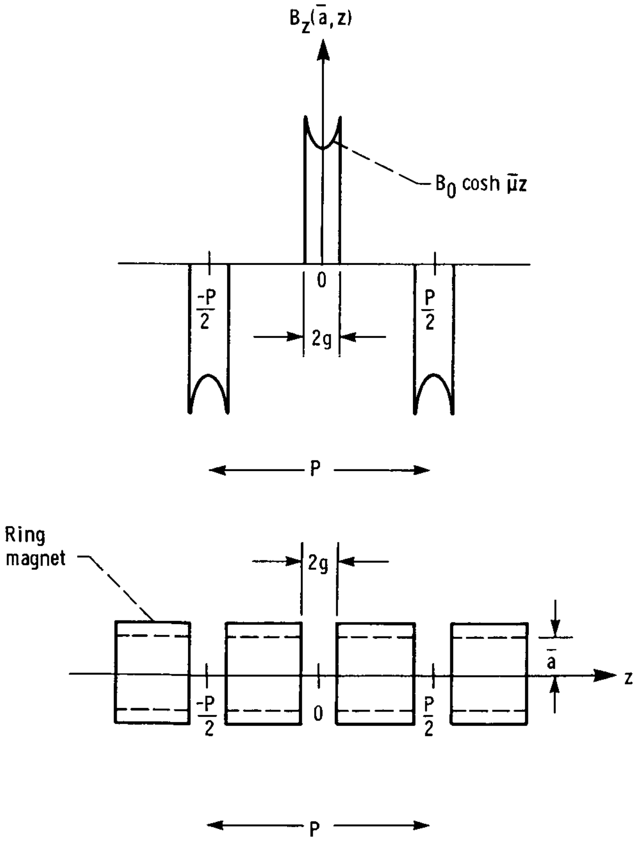

Figure 2.—Geometry and axial magnetic field for single-period PPM focusing.

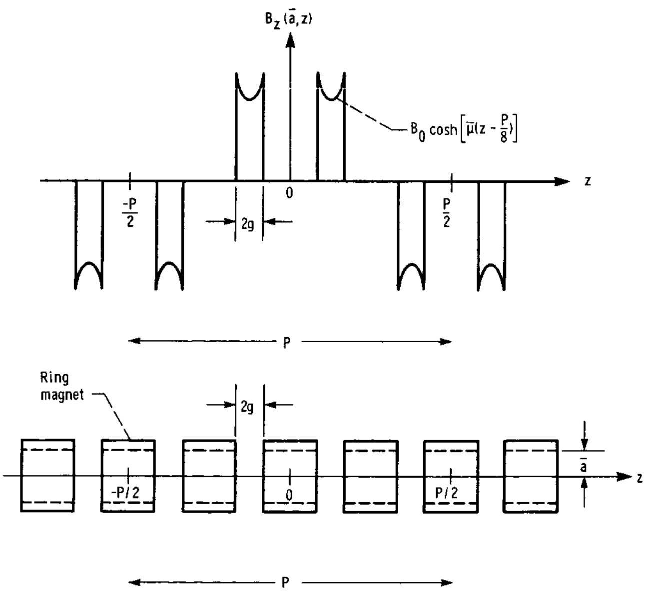

Figure 3.—Geometry and axial magnetic field for double-period PPM focusing.

Figure 3 shows the geometry and axial magnetic field for double-period PPM focusing. The magnetic field is given by equations (21) and (22) with

$$a_n = \begin{cases} \dfrac{2 \cos \dfrac{n\pi}{4} (8B_0) (\bar{\mu} \sinh \bar{\mu} g \cos k_n g + k_n \cosh \bar{\mu} g \sin k_n g)}{P\left(\bar{\mu}^2 + k_n^2\right) I_0(k_n \bar{a})}, & n \text{ odd} \\ 0, & n \text{ even} \end{cases} \tag{25}$$

As before, the measured on-axis values $B_z(0,z)$ over a magnetic period may be entered instead.

Descriptions of the program input parameters are given as follows:

Name	Description
ABARCM	Inner radius, $\bar{a}$, of magnet stack from iron pole piece to tube axis, cm. ABARCM needs to be loaded only if NBZDAT = 0
ACM	Tunnel radius, a, cm
ALPHL(K)	Power attenuation of forward wave in going from cavity K to cavity $K + 1$, dB/cavity; K = 1, LASTCV. To simulate a sever, a large value (e.g., 350 dB) is chosen for ALPHL in the sever cavity
ALPHLR(K)	Power attenuation of backward wave in going from cavity $K + 1$ to cavity K, dB/cavity; K = 1, LASTCV. ALPHLR needs to be loaded only if KLOSS = 1
B0(K)	Axial magnetic field at inner radius of magnet stack and midpoint of gap in K^{th} magnetic section, B_0, T; K = 1, LASTMG. B0(K) needs to be loaded only if NBZDAT = 0
B1LDP(K)	Phase shift of voltage for cavity K divided by π, $(\beta_1 L)_K/\pi$, rad; K = 1, LASTCV
BCM	Initial beam radius, b_0, cm
BZDATA(I)	Experimentally obtained value of axial magnetic field on the axis for NBZDATA equally spaced data points. I = 1 corresponds to the beginning of a magnetic section, and I = NBZDATA + 1 corresponds to the end of a section. BZDATA(I) needs to be loaded only if NBZDAT $\neq$ 0
DRDZ(I)	Initial value of dr/dz for I^{th} ring; I = 1, NRINGS. I = 1 corresponds to the innermost ring
FREQGH	Frequency, GHz
I0BMA	Beam current at tube entrance, I_0, mA
JSCF	Number of integration steps between calculations of space-charge forces
KAV13	Number of the first cavity in the two-dimensional region KAV13 = 1: two-dimensional model KAV13 = LASTCV + 1: one-dimensional model
KIMP	KIMP = 0: Pierce impedance is entered as input in ZIMP KIMP = 1: total impedance is entered as input in ZIMP
KLMAG	KLMAG = 0: cavity lengths and magnetic sections coincide KLMAG = 1: cavity lengths and magnetic sections do not coincide
KLOSS	KLOSS = 0: ALPHLR(K) is set equal to ALPHL(K); thus ALPHLR(K) does not need to be loaded. This is the usual case KLOSS = 1: the backward wave attenuation is given by ALPHLR(K)
KPPM	KPPM = 1: single-period PPM focusing is to be used KPPM = 2: double-period PPM focusing is to be used
KPRINT	KPRINT = 0: print input data KPRINT = 1: do not print input data
KREL	KREL = 0: use relativistic equations of motion KREL = 1: use nonrelativistic equations of motion
KSMSIG	KSMSIG = 0: do not print small-signal parameters KSMSIG = 1: print small-signal parameters
KSPACE	KSPACE = 0: calculate space-charge forces KSPACE = 1: set space-charge forces equal to zero

KSOLEN — KSOLEN = 0: use PPM focusing
KSOLEN = 1: use solenoid focusing; B_z = B0, $B_r = 0$

KVEL(I) — Number of cavity for I[th] printout of normalized axial velocities of rings; I = 1, NVEL

KWRITM — KWRITM = 0: do not print normalized masses of rings
KWRITM = 1: print normalized masses of rings whenever normalized axial velocities of rings are printed

KWRITV — KWRITV = 0: do not print normalized radial velocities of rings
KWRITV = 1: print normalized (to initial axial velocity) radial velocities of rings whenever normalized axial velocities of rings are printed

LASTCV — Number of last cavity (LASTCV ≤ 200)

LASTMG — Number of magnetic sections (LASTMG ≤ 200). A magnetic section is one-half of the magnetic period for single-period PPM focusing and one-fourth of the magnetic period for double-period PPM focusing

LCIRCM(K) — Length of K^{th} cavity, L_K, cm; K = 1, LASTCV

LGAPCM(K) — Length of gap in K^{th} cavity, $2\ell_K$, cm; K = 1, LASTCV

LMAGCM(K) — Length of K^{th} magnetic section, cm; K = 1, LASTMG. LMAGCM(K) needs to be loaded only if KLMAG = 1

MSHAPE(K) — Electric field shape parameter for K^{th} cavity, $\bar{m}$, m^{-1}; K = 1, LASTCV; with ratio

$$\frac{E_z(a, z_{\text{gap edge}})}{E_z(a, z_{\text{gap center}})} = \cosh(\bar{m}\ell) \tag{26}$$

where $\bar{m}$ = MSHAPE(K) and ℓ is half-length in meters of K^{th} cavity gap. (This formulation is discussed in detail in reference 4.) For blunt tunnel tips, MSHAPE = 1

MU(K) — Magnetic field shape parameter for K^{th} magnetic section, $\bar{\mu}$, m^{-1}; K = 1, LASTMG; with ratio

$$\frac{B_z(\bar{a}, z_{\text{gap edge}})}{B_z(\bar{a}, z_{\text{gap center}})} = \cosh(\bar{\mu} g) \tag{27}$$

where $\bar{\mu}$ = MU(K) and g is half-length in meters of K^{th} magnetic gap. MU(K) needs to be loaded only if NBZDAT = 0. For a ratio equal to one, set MU = 1

NBWM — NBWM = 0: no backward wave
NBWM > 0: number of last cavity considered in calculating backward wave

NBZDAT — NBZDAT = 0: magnetic fields are determined by input data B0 and MU
NBZDAT > 0: magnetic fields are determined from experimental data. The number of experimental data values for the axial magnetic field on the axis is NBZDAT + 1 (NBZDAT ≤ 100)

NCAVSS — Number of cavity for which small-signal parameters are calculated

NDISKS — Number of disks in beam wavelength (NDISKS ≤ 24)

NMAX — Number of terms in summations stored in tables, excluding space-charge force tables and magnetic field tables (NMAX ≤ 40)

NPGRID — Number of grid points in radial direction is NPGRID + 1. Refers only to the grid for calculating forces on rings due to electric and magnetic fields (NPGRID ≤ 20)

NPSC — Number of grid points in radial direction is NPSC + 1. Refers only to grid for calculating forces on rings due to space-charge fields (NPSC ≤ 20)

NRINGS — Number of rings per disk (NRINGS ≤ 4)

NVEL — Number of cavities for which ring axial velocities are printed out

NXGRD1 — Number of grid points in axial direction per cavity in one-dimensional region (NXGRD1 ≤ 64). NXGRD1 must be a multiple of four

NXGRD3 — Number of grid points in axial direction per cavity in two-dimensional region (NXGRD3 ≤ 64). NXGRD3 must be a multiple of four

NXMAG — Number of grid points in axial direction per magnetic section (NXMAG ≤ 64, normally the same as NXGRD3). NXMAG must be a multiple of four. NXMAG needs to be loaded only if KLMAG ≠ 0

PCDPA — Cathode flux parameter is the ratio of the magnetic flux linking a disk defined by the beam's radius at the cathode to that linking a disk defined by its radius at the input plane of the interaction region

PINDBM — Input power, P_{in}, dBm

TOLDV — Error criterion for determining whether an additional pass through a cavity is required. If

$$\frac{\Delta V_{f,\text{new}} - \Delta V_{f,\text{old}}}{V_{f,\text{new}}} > \text{TOLDV} \quad (28)$$

then an additional pass is made. Typical value, 0.025

TOLSC	Error criterion for determining whether the frequency of calculating space-charge forces should be doubled (ref. 3). Typical value, 0.025
TOLTBL	Error criterion used in electric and magnetic field tables for determining the number of terms to include in series (ref. 3). Typical value, 0.001
TWOGCM(K)	Length of gap in K^{th} magnetic section, $2g$, cm; K = 1, LASTMG
VOB	Beam voltage, V_0, V
VJUMP(K)	The dc voltage jump for K^{th} cavity, V; K = 1, LASTCV
ZIMP(K)	KIMP = 0: ZIMP(K) is Pierce, or beam-coupling, impedance in ohms for the K^{th} cavity (ref. 5, eq. (10.1.19)); K = 1, LASTCV
	KIMP = 1: ZIMP(K) is the total interaction impedance in ohms for the K^{th} cavity; K = 1, LASTCV. The total interaction impedance for the K^{th} cavity is defined by

$$Z_K = \frac{V_K^2}{2P_{f,K}} \quad (29)$$

where V_K is the amplitude of the voltage across the gap and $P_{f,K}$ is the average power flow in the forward direction

Model Output

The program output includes three parts: the printing of small-signal parameters (if KSMSIG = 1), a cavity-by-cavity printing of selected data, and the printing of data on ring dynamics at selected cavities.

The small-signal parameters (refs. 5 and 6) are as follows:

Name	Description
U0	Initial beam velocity, u_0, m/sec
BEB	Product of beam propagation constant and beam radius, $(\omega/u_0)b_0$, where ω is angular frequency and b_0 is initial beam radius
B1B	Product of wave propagation constant and beam radius, $(\omega/v_p)b_0$, where v_p is wave phase velocity
KP	Pierce impedance, Ω
ZC	Total impedance, Ω
C	Pierce's gain parameter, C
B	Pierce's b, $(u_0 - v_p)/v_pC$
D	Pierce's loss parameter, d
DGAIN	Small-signal gain per cavity, dB/cavity
QC	Pierce's space-charge parameter, QC/C
A1A2	Launching loss, $A_1 + A_2$, dB

The following data are printed for each cavity:

Name	Description
CAV	Cavity number
VMAG	Magnitude of gap voltage, V
ISMAG	Magnitude of induced current normalized to input current
ISPHA	Phase of normalized induced current divided by π, rad
LSGAIN	Large-signal gain, dB
POUT	Output power divided by I_0V_0
AVERHO	Average of the ring centroid radii divided by tunnel radius
RMSANG	Root mean square (RMS) value of the angle that the velocity vectors of the rings make with the axis, deg
RMSVEL	Root mean square (RMS) value of the normalized radial velocities of the rings with respect to the initial axial velocity
PKE	Change in beam kinetic power from initial beam kinetic power divided by I_0V_0
INTRC	Power loss due to beam interception divided by I_0V_0
PRF	Power in forward wave divided by I_0V_0
PBW	Power in backward wave divided by I_0V_0
PLC	Cumulative power loss (except for loss due to beam interception), divided by I_0V_0
PBAL	Power balance equal to

$$1 + \frac{\text{PKE} - \text{PJUMP} + \text{PRF} + \text{PBW} + \text{PLC} + \text{INTRC}}{I_0V_0} \quad (30)$$

where PJUMP is the cumulative power due to all the voltage jumps up to the current cavity

SC	Number of integration steps between calculations of space-charge forces

At selected cavities, the following data are printed:

Normalized axial velocities	Axial velocities normalized with respect to the initial beam velocity
Normalized radial velocities	Radial velocities normalized with respect to the initial beam velocity. Printed only if KWRITV = 1

Normalized ring masses	Ring masses normalized with respect to initial ring mass. Printed only if KWRITM = 1
Ring radius divided by *a*	Ring radii normalized with respect to tunnel radius *a*

Modeling the CTS Tube

To test the model, it was used to simulate the Communications Technology Satellite (CTS) traveling-wave tube (ref. 7), which is a 200-W, 12-GHz TWT with 58 cavities and 3 sections, with the output section containing 3 velocity tapers. The geometric dimensions and electrical parameters from 12.00 to 12.20 GHz in 50-MHz intervals for each of the 58 cavities are given in tables I to IV of reference 1. A sample input dataset and its resulting output are shown in the appendix.

Figure 4 shows the experimental small-signal gain as a function of frequency at 0-dBm input power drive, 11.3-kV cathode voltage, and 71-mA beam current (ref. 1). Connolly and O'Malley compared this curve to that obtained with their one-dimensional model. Their results can be duplicated by setting KAV13 = 59, wherein this model reverts back to one-dimensional. The small-signal gain as a function of frequency both with and without a backward wave included is shown in figure 4. These results duplicate those of Connolly and O'Malley. The results without backward wave are simply those obtained after just one integration pass through the tube. To obtain the results with backward wave, multiple passes through the tube were performed until the solution converged. At the low end of the frequency band there was a significant difference between results with and without backward wave, and approximately ten passes were needed to obtain convergence. Through the rest of the frequency band the backward wave did not make a significant contribution, and only a few passes were needed.

The one-dimensional model with backward wave simulates experimental small-signal gain as a function of frequency very well except for a ripple. It is believed that this ripple was primarily due to wave reflections between the output coupling cavity and the last sever. The model does not presently have the capability to model this reflection.

To utilize the two-dimensional capability of the model, it is necessary to specify the magnetic field. A double-period PPM design is used in which there are four cavities per magnetic period. The inner radius of the iron magnetic pole pieces is equal to that of the tunnel radius and gives ABARCM = ACM = 0.0635. Figure 5 (from ref. 7) shows that the measured magnetic field at the axis was approximately 0.15 T over the first 29 cavities and 0.22 T over the second 29 cavities. For double-period PPM focusing, the program requires that the magnetic field input data be grouped in sections of four. Thus to model this magnetic focusing, the input parameter B0 (which is specified at the inner radius of the magnet stack) was chosen to give a maximum magnetic field at the axis equal to 0.1500 T over the first 28 cavities and equal to 0.2200 T over cavities 29 through 58. To determine the proper value of B0, the ratio between the maximum magnetic field at the magnet stack radius to that at the axis needs to be calculated from

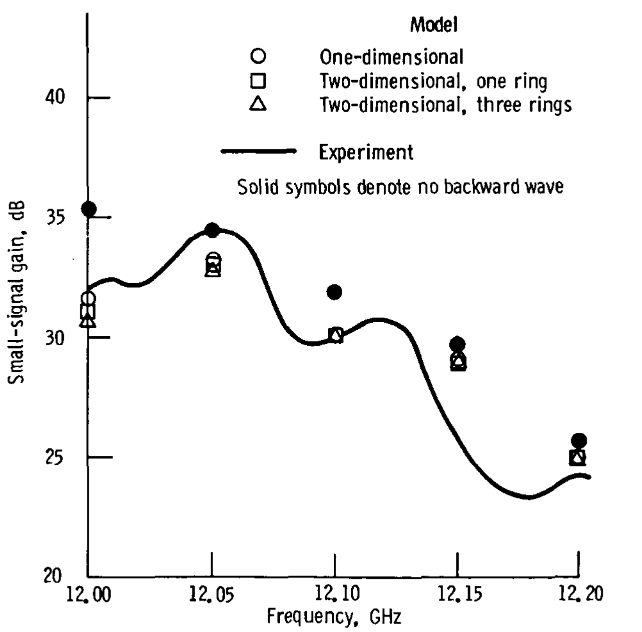

Figure 4.—Model and experimental results for small-signal gain as function of frequency for Communications Technology Satellite traveling-wave tube. (PINDBM = 0, VOB = 11 300, IOBMA = 71.)

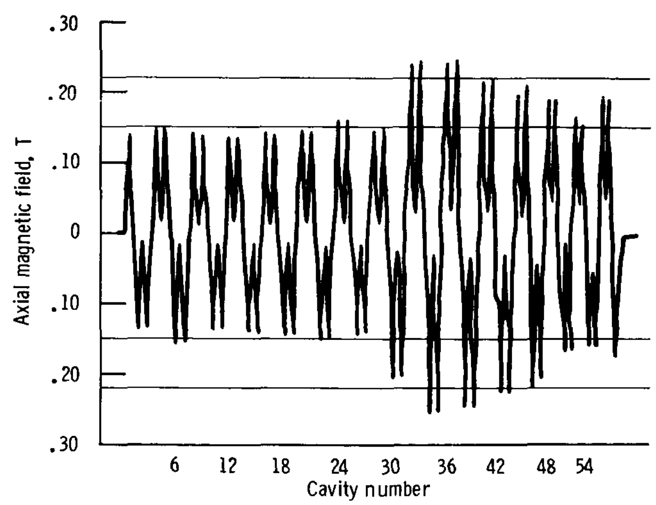

Figure 5.—Experimental axial magnetic field at axis of Communications Technology Satellite traveling-wave tube (from ref. 6).

$$\frac{B_0(r = \bar{a}, z = \text{gap center})}{B_z(r = 0, z = \text{gap center})} = \frac{\sum_{n=1}^{\infty} a_n I_0(k_n \bar{a})}{\sum_{n=1}^{\infty} a_n} \tag{31}$$

where a_n is determined from equation (24). For this tube the ratio is 1.25, and thus the input is determined to be 0.1875 T for the first 28 sections and 0.2750 T for the next 30 sections (B0 = 28*0.1875, 30*0.2750).

With the above magnetic field specifications, the two-dimensional model was run at small signal (PINDBM = 0) with both one ring and three rings (fig. 4). Results for both one and three rings were virtually identical to that for the one-dimensional model. This gives confidence that the model code is error free and also indicates that the one-dimensional model is adequate to determine the small-signal gain.

Next, results at saturation at the center frequency of 12.10 GHz were compared. To determine the input power needed for saturation, runs were made scanning power input (PINDBM) with the one-dimensional specification. The resulting efficiency as a function of input power plot of figure 6 indicates that saturation occurs for an input power of 24 dBm. This compares well with the experimentally obtained value of 23 dBm.

At saturation (PINDBM = 24), the two-dimensional model with one, two, three, and four rings was compared with the one-dimensional model and experimental data, and the results are shown in table I. The results from all the models compare well with experiment in gain and beam efficiency. The experimental results indicate an interception of 6 percent, whereas the two-dimensional models have only 1-percent interception. This is probably because thermal electrons were not taken into account.

TABLE I.—GAIN, BEAM EFFICIENCY, AND INTERCEPTION FOR ONE- AND TWO-DIMENSIONAL MODELS AND EXPERIMENT

[CTS TWT at saturation at 12.10 GHz.]

Model	Gain, dB	Beam efficiency, percent	Interception, percent
One-dimensional	29.4	27.3	0
Two-dimensional			
One ring	28.8	23.6	1
Two rings	28.8	24.0	1
Three rings	28.8	23.8	1
Four rings	29.0	24.9	1
Experiment	30.4	24.9	6

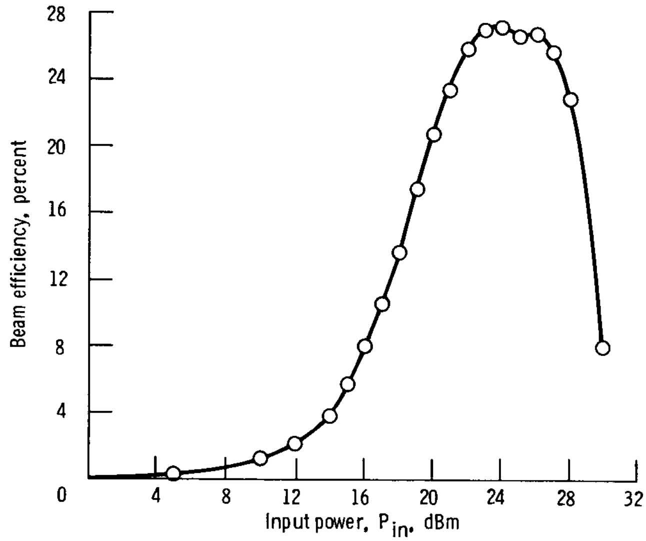

Figure 6.—Beam efficiency as function of input power for one-dimensional model with backward wave at frequency 12.10 GHz for Communications Technology Satellite traveling-wave tube.

A small decrease occurs in both the gain and efficiency in going from the one- to two-dimensional model. This is primarily due to the beam interception in the two-dimensional model. There is virtually no difference among the results with one, two, and three rings. This gives added confidence that the code is error free and indicates that the one-ring model is adequate for modeling the two-dimensional electron trajectories. The accuracy is only minimally improved by increasing the number of rings.

Conclusions

The NASA large-signal, two-dimensional computer model for a coupled-cavity traveling-wave tube was described, and details of specifying the input were given. The model was tested by comparing its results to those of the one-dimensional model and experimental data for the CTS TWT. The agreement was excellent at both small-signal and saturation.

It was found that the one-ring, two-dimensional model gave very good results, and accuracy was not improved measurably when more rings were used. Although the one-dimensional model is adequate for calculating gain and efficiency, the two-dimensional model computes the trajectories necessary for designing the magnetic focusing and calculating the beam entrance conditions required for multistage collector design.

Lewis Research Center
National Aeronautics and Space Administration
Cleveland, Ohio, October 28, 1986

Appendix—Sample Dataset for CTS TWT at 12.10 GHz

Input

This input dataset corresponds to the two-dimensional, one-ring run at 12.10 GHz of figure 4. The number of passes is controlled by the number of "&INPUT &END" lines at the end. A negative value of ACM causes the program to terminate. As written, this file makes five passes through the tube. Changing KAV13 to 59 results in one-dimensional calculations.

```
&INPUT
ABARCM=.0635,
ACM=.0635,
ALPHL=2*0.1,7*.06,2*.1,350.,2*.1,11*.06,2*.1,350.,2*.1,
9*.06,4*.065,2*.07,.075,5*.08,.09,.1,2*.11,3*.1,
B0=28*.1875,30*.275,
B1LDP=1.51,1.36,7*1.23,1.36,3*1.51,1.36,11*1.23,1.36,3*1.51,
1.36,9*1.23,3*1.25,5*1.25,9*1.24,1.36,1.51,
BCM=.03175,
DRDZ=4*0.0,
FREQGH=12.10,
IOBMA=71.0,
JSCF=1,
KAV13=1,
KIMP=1,
KLMAG=0,
KLOSS=0,
KPPM=2,
KPRINT=0,
KREL=0,
KSMSIG=0,
KSPACE=0,
KSOLEN=0,
KVEL=58,
KWRITM=1,
KWRITV=1,
LASTCV=58,
LASTMG=58,
LCIRCM=39*0.3175,3*0.3048,0.2985,0.2921,0.2794,0.2667,
5*0.2540,0.2413,0.2286,5*0.2159,
LGAPCM=39*0.0965,3*0.0914,0.0899,0.0879,0.0843,0.0808,
5*0.0772,0.0739,0.0701,5*0.0660,
MSHAPE=58*1.,
```

```
MU=58*1.,
NBWM=58,
NBZDAT=0,
NCAVSS=1,
NDISKS=24,
NMAX=40,
NPGRID=20,
NPSC=20,
NRINGS=1,
NVEL=1,
NXGRD1=16,
NXGRD3=16,
NXMAG=16,
PCDPA=0.,
PINDBM=0.,
TOLDV=.025,
TOLSC=.025,

TOLTBL=1.E-03,
TWOGCM=39*0.0965,3*0.0914,0.0899,0.0879,0.0843,0.0808,
5*0.0772,0.0739,0.0701,5*0.0660,
VOB=11300.,
VJUMP=58*0.,
ZIMP=400.,780.,1375.,6*1725.,1375.,
780.,2*400.,780.,1375.,10*1725.,1375.,780.,2*400.,780.,
1375.,8*1725.,3*1795.,1710.,1620.,1530.,1440.,5*1350.,
1240.,1130.,2*1015.,810.,500.,300.    &END

&INPUT &END
&INPUT &END
&INPUT &END
&INPUT &END
&INPUT &END
&INPUT ACM=-1000. &END
```

Output After Fifth Pass

ORIGINAL PAGE IS
OF POOR QUALITY

CAV	VMAG	ISMAG	ISPHA	LS GAIN	POUT	AVERHO	RMSANG	RMSVEL	PKE	INTRC	PRF	PBW	PLC	PBAL	SC
1	0.82220E+00	0.0000	-0.8377	-0.0011	0.0000	0.3485	0.0063	0.0020	0.0000	0.0000	0.0000	0.0000	0.0000	1.000	1
2	0.13366E+01	0.0001	0.1510	-0.0920	0,0000	0.3345	0.0112	0.0036	-0.0001	0.0000	0.0000	0.0000	0.0000	1.000	1
3	0.15219E+01	0.0003	0.8426	-0.1409	0.0000	0.3148	0.0132	0.0042	-0.0002	0.0000	0.0000	0.0000	0.0000	1.000	1
4	0.17207E+01	0.0007	-0.4550	-0.1109	0.0000	0.2943	0.0122	0.0039	-0.0003	0.0000	0.0000	0.0000	0.0000	1.000	1
5	0.19282E+01	0.0012	0.2624	-0.0537	0.0000	0.2775	0.0085	0.0027	-0.0005	0.0000	0.0000	0.0000	0.0000	1.000	1
6	0.19443E+01	0.0019	0.9943	0.0351	0.0000	0.2690	0.0020	0.0006	-0.0005	0.0000	0.0000	0.0000	0.0000	0.999	1
7	0.17384E+01	0.0029	-0.2629	0.1858	0.0000	0.2714	0.0051	0.0016	-0.0005	0.0000	0.0000	0.0000	0.0000	1.000	1
8	0.17489E+01	0.0040	0.4863	0.4528	0.0000	0.2841	0.0106	0.0034	-0.0004	0.0000	0.0000	0.0000	0.0000	1.000	1
9	0.20751E+01	0.0052	-0.7638	0.9003	0.0000	0.3031	0.0131	0.0042	-0.0003	0.0000	0.0000	0.0000	0.0000	1.000	1
10	0.19957E+01	0.0066	-0.0136	1.4966	0.0000	0.3239	0.0128	0.0041	-0.0002	0.0000	0.0000	0.0000	0.0000	1.000	1
11	0.16518E+01	0.0081	0.7353	2.3989	0.0000	0.3418	0.0094	0.0030	-0.0001	0.0000	0.0000	0.0000	0.0000	1.000	1
12	0.14358E+01	0.0096	-0.5157	3.2458	0.0000	0.3523	0.0037	0.0012	0.0000	0.0000	0.0000	0.0000	0.0000	1.000	1
13	0.43992E+00	0.0111	0.2332	-15.0619	0.0000	0.3530	0.0028	0.0009	0.0000	0.0000	0.0000	0.0000	0.0000	1.000	1
14	0.74020E+00	0.0124	0.9827	-7.6348	0.0000	0.3439	0.0087	0.0028	-0.0001	0.0000	0.0000	0.0000	0.0000	1.000	1
15	0.11171E+01	0.0137	-0.2660	-2.2815	0.0000	0.3269	0.0125	0.0040	-0.0002	0.0000	0.0000	0.0000	0.0000	1.000	1
16	0.29457E+01	0.0147	0.4852	1.8465	0.0000	0.3062	0.0132	0.0042	-0.0003	0.0000	0.0000	0.0000	0.0000	1.000	1
17	0.44361E+01	0.0153	-0.7646	4.7670	0.0000	0.2868	0.0110	0.0035	-0.0004	0.0000	0.0000	0.0000	0.0000	1.000	1
18	0.49053E+01	0.0157	-0.0237	6.9891	0.0000	0.2730	0.0060	0.0019	-0.0005	0.0000	0.0000	0.0000	0.0000	1.000	1
19	0.49248E+01	0.0160	0.7105	8.7681	0.0000	0.2690	0.0011	0.0003	-0.0005	0.0000	0.0000	0.0000	0.0000	0.999	1
20	0.61483E+01	0.0163	-0.5639	10.2349	0.0000	0.2761	0.0077	0.0025	-0.0005	0.0000	0.0000	0.0000	0.0000	1.000	1
21	0.79287E+01	0.0167	0.1524	11.4695	0.0000	0.2920	0.0119	0.0038	-0.0004	0.0000	0.0000	0.0000	0.0000	1.000	1
22	0.85851E+01	0.0174	0.8552	12.5173	0.0000	0.3122	0.0133	0.0042	-0.0003	0.0000	0.0000	0.0000	0.0000	1.000	1
23	0.83668E+01	0.0191	-0.4469	13.4437	0.0000	0.3323	0.0117	0.0037	-0.0001	0.0000	0.0000	0.0000	0.0000	1.000	1
24	0.92377E+01	0.0218	0.2524	14.2926	0.0000	0.3475	0.0071	0.0023	-0.0001	0.0000	0.0000	0.0000	0.0000	1.000	1
25	0.11131E+02	0.0256	0.9587	15.1155	0.0000	0.3540	0.0011	0.0004	0.0000	0.0000	0.0000	0.0000	0.0000	1.000	1
26	0.10635E+02	0.0306	-0.3295	15.8512	0.0000	0.3505	0.0054	0.0017	-0.0001	0.0000	0.0000	0.0000	0.0000	1.000	1
27	0.85624E+01	0.0366	0.3916	16.6654	0.0001	0.3378	0.0105	0.0033	-0.0002	0.0000	0.0001	0.0000	0.0001	1.000	1
28	0.72345E+01	0.0432	-0.8805	17.3924	0.0001	0.3188	0.0130	0.0041	-0.0003	0.0000	0.0001	-0.0001	0.0001	1.000	1
29	0.91412E+01	0.0494	-0.1487	-2.1107	0.0000	0.2781	0.0376	0.0119	-0.0005	0.0000	0.0000	-0.0001	0.0002	1.000	1
30	0.14036E+02	0.0544	0.5874	5.3045	0.0000	0.2099	0.0464	0.0148	-0.0011	0.0000	0.0000	-0.0001	0.0002	0.999	1
31	0.10259E+02	0.0598	-0.6775	10.6878	0.0000	0.1459	0.0313	0.0100	-0.0017	0.0000	0.0000	-0.0002	0.0002	0.998	1
32	0.22153E+02	0.0647	0.0699	14.8043	0.0000	0.1249	0.0063	0.0020	-0.0020	0.0000	0.0000	-0.0002	0.0002	0.998	1
33	0.36047E+02	0.0660	0.8184	17.6534	0.0001	0.1629	0.0388	0.0123	-0.0016	0.0000	0.0001	-0.0001	0.0002	0.999	1
34	0.33862E+02	0.0650	-0.4505	19.7511	0.0001	0.2323	0.0459	0.0146	-0.0010	0.0000	0.0001	-0.0001	0.0002	0.999	1
35	0.11928E+02	0.0660	0.2654	21.4240	0.0002	0.2947	0.0311	0.0099	-0.0006	0.0000	0.0002	-0.0002	0.0002	1.000	1
36	0.22912E+02	0.0686	0.9831	22.8286	0.0002	0.3229	0.0041	0.0013	-0.0005	0.0000	0.0002	-0.0002	0.0002	1.000	1
37	0.48434E+02	0.0696	-0.3062	23.9874	0.0003	0.3063	0.0247	0.0079	-0.0007	0.0000	0.0003	-0.0001	0.0002	1.000	1
38	0.49826E+02	0.0718	0.3832	24.9305	0.0004	0.2509	0.0438	0.0139	-0.0012	0.0000	0.0004	-0.0001	0.0002	0.999	1
39	0.25493E+02	0.0809	-0.9302	25.7540	0.0005	0.1800	0.0430	0.0137	-0.0018	0.0000	0.0005	-0.0002	0.0003	0.999	1
40	0.30007E+02	0.0948	-0.1995	26.6363	0.0006	0.1311	0.0180	0.0057	-0.0025	0.0000	0.0006	-0.0002	0.0003	0.998	1
41	0.64522E+02	0.1084	0.5632	27.6729	0.0007	0.1330	0.0205	0.0065	-0.0027	0.0000	0.0007	-0.0001	0.0003	0.998	1
42	0.68061E+02	0.1249	-0.6787	28.8200	0.0009	0.1847	0.0442	0.0141	-0.0024	0.0000	0.0009	-0.0001	0.0003	0.999	1
43	0.44037E+02	0.1472	0.0948	30.0640	0.0013	0.2526	0.0444	0.0141	-0.0020	0.0000	0.0013	-0.0002	0.0003	0.999	1
44	0.62202E+02	0.1723	0.9014	31.3741	0.0017	0.3059	0.0275	0.0088	-0.0020	0.0000	0.0017	-0.0003	0.0003	1.000	1
45	0.97813E+02	0.1954	-0.2530	32.6210	0.0023	0.3299	0.0077	0.0025	-0.0026	0.0000	0.0023	-0.0002	0.0004	1.000	1
46	0.10238E+03	0.2146	0.6382	33.6258	0.0029	0.3241	0.0159	0.0051	-0.0035	0.0000	0.0029	-0.0001	0.0004	1.000	1
47	0.82403E+02	0.2301	-0.4240	34.1664	0.0033	0.2937	0.0324	0.0103	-0.0041	0.0000	0.0033	0.0000	0.0004	1.000	1
48	0.80819E+02	0.2419	0.5402	34.0884	0.0032	0.2465	0.0412	0.0131	-0.0042	0.0000	0.0032	-0.0002	0.0005	0.999	1
49	0.96046E+02	0.2484	-0.4895	33.3551	0.0027	0.1953	0.0381	0.0121	-0.0040	0.0000	0.0027	-0.0004	0.0006	0.999	1
50	0.89713E+02	0.2487	0.4895	31.9549	0.0020	0.1563	0.0216	0.0068	-0.0035	0.0000	0.0020	-0.0006	0.0006	0.998	1
51	0.49928E+02	0.2427	-0.5235	30.2004	0.0013	0.1453	0.0057	0.0018	-0.0030	0.0000	0.0013	-0.0006	0.0007	0.998	1
52	0.15088E+02	0.2319	0.4932	29.3929	0.0011	0.1650	0.0275	0.0087	-0.0028	0.0000	0.0011	-0.0005	0.0007	0.999	1
53	0.58935E+02	0.2197	-0.4409	30.3882	0.0014	0.2053	0.0414	0.0132	-0.0028	0.0000	0.0014	-0.0003	0.0007	0.999	1
54	0.75847E+02	0.2074	0.6686	31.5278	0.0018	0.2523	0.0447	0.0142	-0.0030	0.0000	0.0018	-0.0002	0.0008	0.999	1
55	0.67843E+02	0.1944	-0.2064	31.6560	0.0018	0.2981	0.0393	0.0125	-0.0029	0.0000	0.0018	-0.0001	0.0008	1.000	1
56	0.41894E+02	0.1788	0.9095	30.8494	0.0015	0.3340	0.0274	0.0087	-0.0025	0.0000	0.0015	0.0000	0.0009	1.000	1
57	0.27019E+02	0.1624	0.0196	30.0280	0.0013	0.3548	0.0116	0.0037	-0.0022	0.0000	0.0013	0.0000	0.0009	1.000	1
58	0.25125E+02	0.1493	-0.8767	30.0613	0.0013	0.3568	0.0078	0.0025	-0.0022	0.0000	0.0013	0.0000	0.0009	1.000	1

NORMALIZED AXIAL VELOCITIES

1.01165	1.01154	1.01053	1.00867	1.00639	1.00385	1.00111	0.99819	0.99521	0.99240	0.98994	0.98797
0.98646	0.98579	0.98621	0.98772	0.98994	0.99295	0.99635	1.00010	1.00369	1.00671	1.00916	1.01076

NORMALIZED RADIAL VELOCITIES

-0.00281	-0.00301	-0.00303	-0.00307	-0.00298	-0.00294	-0.00328	-0.00370	-0.00390	-0.00375	-0.00335	-0.00271
-0.00191	-0.00124	-0.00064	-0.00033	-0.00030	-0.00038	-0.00064	-0.00113	-0.00158	-0.00189	-0.00211	-0.00242

NORMALIZED RING MASSES

1.00000	1.00000	1.00000	1.00000	1.00000	1.00000	1.00000	1.00000	1.00000	1.00000	1.00000	1.00000
1.00000	1.00000	1.00000	1.00000	1.00000	1.00000	1.00000	1.00000	1.00000	1.00000	1.00000	1.00000

RING RADIUS DIVIDED BY A

0.33865	0.34001	0.34098	0.34370	0.34779	0.34841	0.35167	0.35834	0.36430	0.36950	0.37477	0.37988
0.38115	0.38544	0.38178	0.37415	0.36707	0.36024	0.35260	0.34568	0.34132	0.33889	0.33856	0.33864

References

1. Connolly, D.J.; and O'Malley, T.A.: Computer Program for Analysis of Coupled-Cavity Traveling-Wave Tubes. NASA TN D-8492, 1977.
2. O'Malley, T.A.; and Connolly, D.J.: Users' Manual for Computer Program for One-Dimensional Analysis of Coupled-Cavity Traveling-Wave Tubes. NASA TM X-3565, 1977.
3. O'Malley, T.A.: User's Manual for Computer Program for Three-Dimensional Analysis of Coupled-Cavity Traveling-Wave Tubes. NASA CR-168269, 1984.
4. Kosmahl, H.G.; and Branch, G.M., Jr.: Generalized Representation of Electric Fields in Interaction Gaps of Klystrons and Traveling-Wave Tubes. IEEE Trans. Electron Devices, vol. 20, no. 7, July 1973, pp. 621-629.
5. Gewartowski, J.W.; and Watson, H.A.: Principles of Electron Tubes. Van Nostrand, 1965.
6. Pierce, J.R.: Traveling-Wave Tubes. Van Nostrand, 1950.
7. Jones, C.L.: A 200 Watt Traveling-Wave-Tube for the Communications Technology Satellite. NASA CR-135029, 1976.

1. Report No. NASA TP-2675	2. Government Accession No.	3. Recipient's Catalog No.
4. Title and Subtitle Revised NASA Axially Symmetric Ring Model for Coupled-Cavity Traveling-Wave Tubes		5. Report Date January 1987
		6. Performing Organization Code 506-44-21
7. Author(s) Jeffrey D. Wilson		8. Performing Organization Report No. E-3220
		10. Work Unit No.
9. Performing Organization Name and Address National Aeronautics and Space Administration Lewis Research Center Cleveland, Ohio 44135		11. Contract or Grant No.
		13. Type of Report and Period Covered Technical Paper
12. Sponsoring Agency Name and Address National Aeronautics and Space Administration Washington, D.C. 20546		14. Sponsoring Agency Code

15. Supplementary Notes

16. Abstract

A versatile large-signal, two-dimensional computer program is used by NASA to model coupled-cavity traveling-wave tubes (TWT's). In this model, the electron beam is divided into a series of disks, each of which is further divided into axially symmetric rings which can expand and contract. The trajectories of the electron rings and the radiofrequency (RF) fields are determined from the calculated axial and radial space-charge, RF, and magnetic forces as the rings pass through a sequence of cavities. By varying electrical and geometric properties of individual cavities, the model is capable of simulating severs, velocity tapers, and voltage jumps. The calculated electron ring trajectories can be used in designing magnetic focusing and multidepressed collectors. The details of using the program are presented, and results are compared with experimental data.

17. Key Words (Suggested by Author(s)) Coupled-cavity Traveling-wave tubes Computer model	18. Distribution Statement Unclassified – unlimited STAR Category 33

19. Security Classif. (of this report)	20. Security Classif. (of this page)	21. No of pages	22. Price*
Unclassified	Unclassified	16	A02

*For sale by the National Technical Information Service, Springfield, Virginia 22161